

Large-Scale Cortical Networks for Hierarchical Prediction and Prediction Error in the Primate Brain

Highlights

- A data-driven analysis (PARAFAC) recovers prediction and prediction-error signals
- Prediction and prediction-error signals arise from different cortical areas
- Gamma and alpha/beta bands convey distinct prediction and prediction-error signals
- Prefrontal cortex sends signals to temporal cortex to update next-trial predictions

Authors

Zenas C. Chao, Kana Takaura,
Liping Wang, Naotaka Fujii,
Stanislas Dehaene

Correspondence

zenas.c.chao@gmail.com

In Brief

Predictive-coding theory proposes that the brain acts as a predictor of sensory inputs. Using high-density ECoG in monkeys, Chao et al. test its core hypothesis by identifying prediction and prediction-errors signals at two different hierarchical levels and examining their interactions.

Large-Scale Cortical Networks for Hierarchical Prediction and Prediction Error in the Primate Brain

Zenas C. Chao,^{1,2,7,*} Kana Takaura,² Liping Wang,³ Naotaka Fujii,^{2,6} and Stanislas Dehaene^{4,5,6}

¹Department of Neuroscience, Graduate School of Medicine and Faculty of Medicine, Kyoto University, Kyoto 6068501, Japan

²RIKEN Brain Science Institute, Wako, Saitama 3510198, Japan

³Institute of Neuroscience, Shanghai Institutes for Biological Sciences, Chinese Academy of Sciences, Shanghai 200031, China

⁴Cognitive Neuroimaging Unit, CEA DSV/I2BM, INSERM, Université Paris-Sud, Université Paris-Saclay, NeuroSpin Center, 91191 Gif/Yvette, France

⁵Collège de France, Paris 75005, France

⁶Senior author

⁷Lead Contact

*Correspondence: zenas.c.chao@gmail.com

<https://doi.org/10.1016/j.neuron.2018.10.004>

SUMMARY

According to predictive-coding theory, cortical areas continuously generate and update predictions of sensory inputs at different hierarchical levels and emit prediction errors when the predicted and actual inputs differ. However, predictions and prediction errors are simultaneous and interdependent processes, making it difficult to disentangle their constituent neural network organization. Here, we test the theory by using high-density electrocorticography (ECoG) in monkeys during an auditory “local-global” paradigm in which the temporal regularities of the stimuli were controlled at two hierarchical levels. We decomposed the broadband data and identified lower- and higher-level prediction-error signals in early auditory cortex and anterior temporal cortex, respectively, and a prediction-update signal sent from prefrontal cortex back to temporal cortex. The prediction-error and prediction-update signals were transmitted via γ (>40 Hz) and α/β (<30 Hz) oscillations, respectively. Our findings provide strong support for hierarchical predictive coding and outline how it is dynamically implemented using distinct cortical areas and frequencies.

INTRODUCTION

The predictive-coding theory states that the brain constantly learns statistical regularities in the sensory environment and actively generates predictions that are confronted to incoming sensory inputs (Friston, 2005; Mumford, 1992; Rao and Ballard, 1999; Srinivasan et al., 1982). This is achieved by a bidirectional cascade of cortical processes, where higher-level structures attempt to predict inputs from lower-level ones through top-

down connections, and error signals are sent back through bottom-up connections in order to update the internal models that lead to those predictions. This hierarchical predictive-coding framework offers a unified model of perception, action, and attention (Clark, 2013; Friston, 2010), and even possibly psychiatric disorders such as schizophrenia and autism (Quattrocki and Friston, 2014; Stephan et al., 2009).

The predictive-coding theory has been supported by a wide range of evidence, which primarily demonstrates the effects of a top-down prediction on facilitating behavioral and neural responses in visual perception (Egner et al., 2010; Kok et al., 2012; Summerfield et al., 2006; Summerfield and Koechlin, 2008), auditory perception (Todorovic et al., 2011), and audiovisual speech perception (Blank and Davis, 2016). However, one core hypothesis derived from the predictive-coding model has not yet been directly evaluated: the existence of simultaneous and interdependent computations of predictions and prediction errors, carried out by distinct and hierarchically organized neuronal populations (as proposed by Friston, 2005), and transmitted between hierarchical levels via cortical oscillations of distinct frequency channels (as proposed by Arnal and Giraud, 2012; Bastos et al., 2012; Wang, 2010). Recent studies have shown that bottom-up and top-down signaling utilizes different frequency channels in both visual processing (Bastos et al., 2015b; Michalareas et al., 2016; van Kerkoerle et al., 2014) and auditory processing (Dürschmid et al., 2016; Fontolan et al., 2014; Sedley et al., 2016), but it remains unclear what kind of information is carried in these frequency channels (in the predictive coding perspective) and how they influence each other. Here, we specifically set out to evaluate the hypothesis by identifying comprehensive dynamics of prediction and prediction-error signals and examine their interactions across hierarchies and frequencies.

Empirically, prediction-error signals have been linked to neural activity evoked by unexpected or novel stimuli, which has been detected at both the macroscopic level (Alink et al., 2010; Binkshstein et al., 2009; Egner et al., 2010; El Karoui et al., 2014; Todorovic et al., 2011; Wacongne et al., 2011) and the

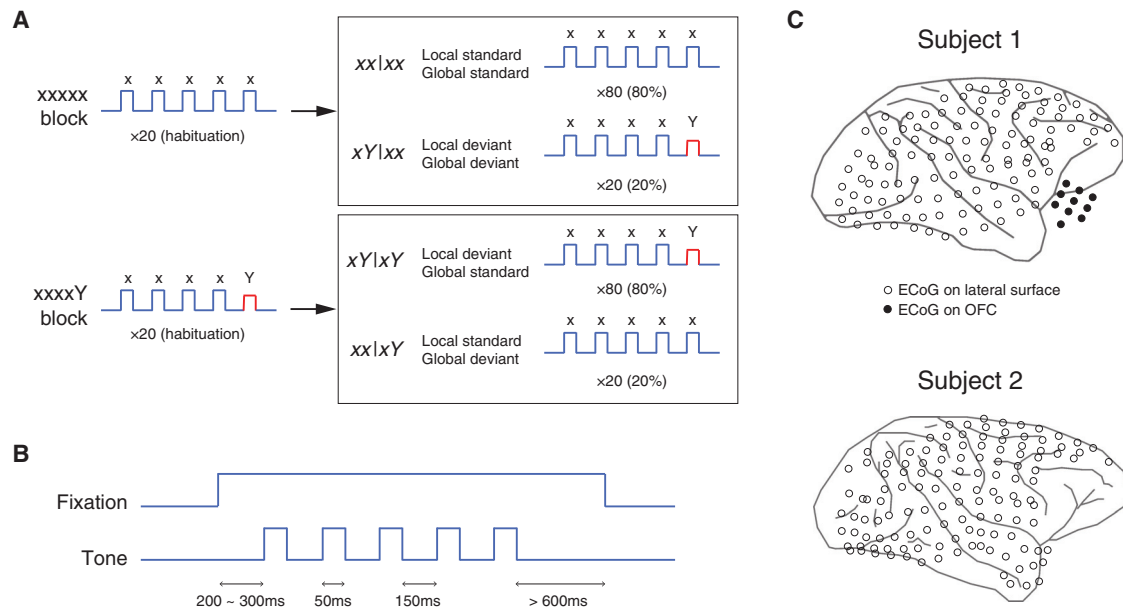


Figure 1. Local-Global Paradigm and Experimental Setup

- (A) The local-global paradigm.
 (B) Sound sequence and task design.
 (C) ECoG electrodes layout.

microscopic level (Eliades and Wang, 2008; Keller et al., 2012). To evaluate the hierarchical organization of prediction-error signals, an auditory paradigm named the “local-global” paradigm was created (Bekinschtein et al., 2009), which introduces two types of temporal regularities (tone-to-tone transition probability versus overall multi-tone sequence) and uses their violations to probe novelty responses at two distinct levels of the cortical hierarchy (Figure 1). The paradigm has been used to investigate hierarchical auditory processing in humans and non-human primates (El Karoui et al., 2014; Strauss et al., 2015; Uhrig et al., 2014; Wacongne et al., 2011; Wang et al., 2015); however, the precise contributions of prediction and prediction-error signals in the hierarchical novelty responses remain unclear, due to the challenge of unwinding the underlying network dynamics that are not only simultaneous and interdependent, but also spatially dispersed and temporally fine-tuned.

To overcome the challenge, we combined the auditory local-global paradigm with large-scale neurophysiological recordings in non-human primates and their automatized analysis by an objective decomposition method (Chao et al., 2015). We used an electrocorticography (ECoG) system to acquire high-fidelity broadband neuronal signals from an entire cortical hemisphere with balanced spatial, spectral, and temporal resolutions (Chao et al., 2010, 2015; Fukushima et al., 2015; Yanagawa et al., 2013). After obtaining this large-scale database of cortical activity, we used an unbiased data-driven analytical approach to search for multiple, possibly superimposed, time-frequency components in large-scale network dynamics (Chao et al., 2015, 2018), and further tested whether their functional profiles and their trial-by-trial interactions fit with the predictive-coding framework.

Specifically, the predictive-coding framework predicted that (1) violations of local transition probability would arise early on, in a bottom-up manner, from early auditory cortex; (2) violations of the overall sequence would arise later, still in a bottom-up manner, from higher-order cortices; (3) the latter violations would require revising the mental representation of the sequence in the higher-level system, thought to involve the prefrontal cortex (PFC) (Bekinschtein et al., 2009; Chennu et al., 2013; El Karoui et al., 2014; Uhrig et al., 2014; Wacongne et al., 2011), and sending top-down messages updating the predictions for the next trial in lower-level sensory areas. Furthermore, our design offered a novel means of testing the hypothesis that bottom-up and top-down cortical signaling is achieved, respectively, by message-passing in γ versus α/β frequency bands.

RESULTS

Local-Global Paradigm to Establish Hierarchical Auditory Regularities

Two macaque monkeys, identified as subjects 1 and 2, were used in this study. During the task, monkeys listened passively to a series of short sound sequences based on the local-global auditory paradigm (Figure 1A). To ensure vigilance, monkeys were required to fixate during each trial (Figure 1B). Cortical activity was recorded with a 128-channel ECoG array covering nearly an entire right cerebral hemisphere (Figure 1C).

On each trial, a series of 5 tones were delivered (Figure 1A). The first 4 tones were identical, either low pitched (tone A) or high pitched (tone B), but the fifth tone could be either the same (AAAAA or BBBBB, jointly denoted by xxxxx) or different

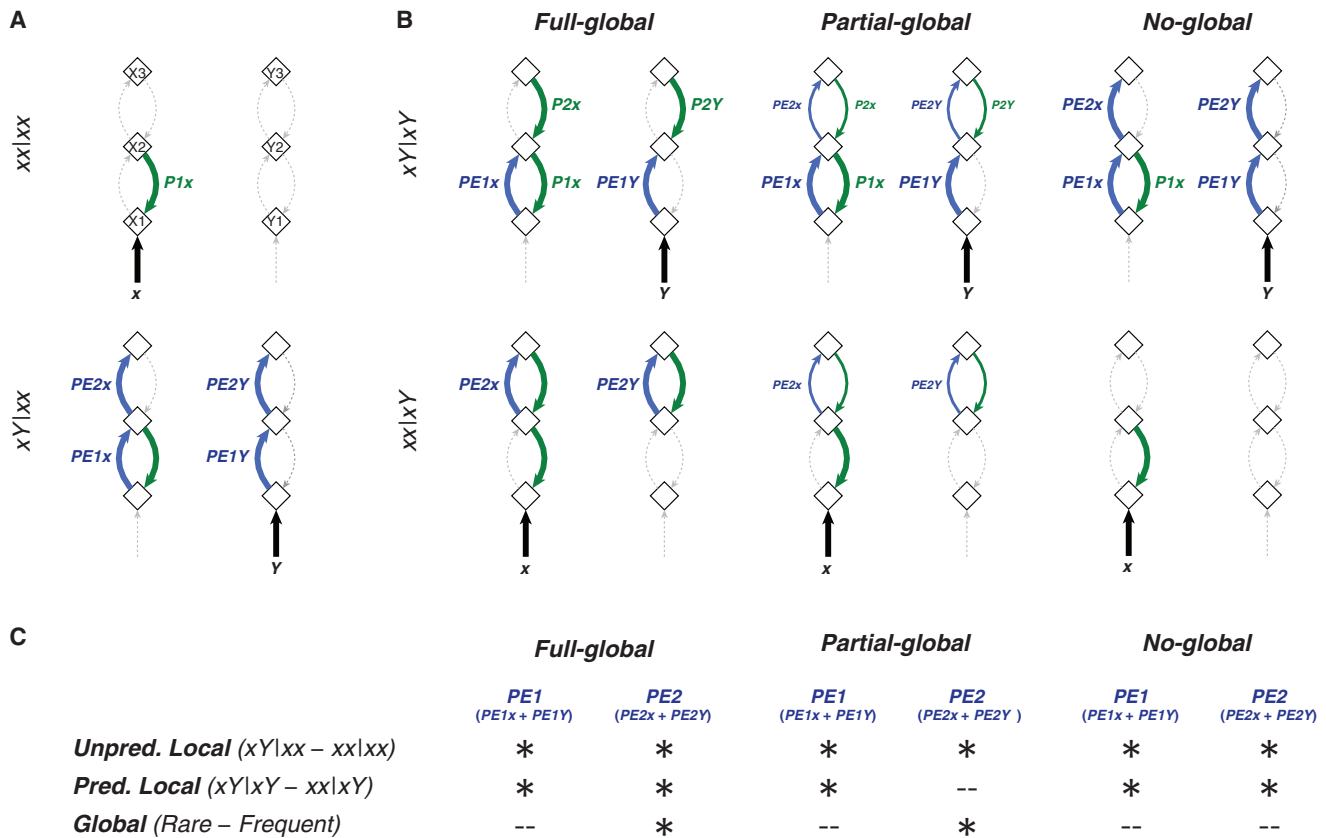


Figure 2. A Predictive-Coding Model of the Local-Global Paradigm

(A) Proposed neural processes in xxxxx blocks. Two hierarchical neuronal populations are shown: one for processing local standard tone x (population X: X1, X2, and X3), and the other for processing local deviant tone Y (population Y: Y1, Y2, and Y3). On $xx|xx$ trials (top), the fifth tone x (black arrow) is predicted by $P1x$ (green arrow), and thus no prediction error should be generated. On $xY|xx$ trials (bottom), $PE1x$ and $PE1Y$ (blue arrows) occur and propagate to the higher level ($PE2x$ and $PE2Y$).

(B) Left: Neural processes in xxxxY blocks in *Full-global*. On $xY|xY$ trials, $PE1x$ and $PE1Y$ appear but are fully predicted by $P2x$ and $P2Y$. On $xx|xY$ trials, $PE2x$ and $PE2Y$ appear, since $PE1x$ and $PE1Y$ expected by $P2x$ and $P2Y$ are mostly omitted. Middle: xxxxY blocks in *Partial-global*. Compared with *Full-global*, the reduced $P2x$ and $P2Y$ induce $PE2x$ and $PE2Y$ on $xY|xY$ trials and reduce $PE2x$ and $PE2Y$ on $xx|xY$ trials. Right: xxxxY blocks in *No-global*. Without global predictions, processes on $xY|xY$ and $xx|xY$ trials are identical to those on $xY|xx$ and $xx|xx$ trials, respectively.

(C) Appearance profiles of $PE1$ ($PE1x$ and $PE1Y$) and $PE2$ ($PE2x$ and $PE2Y$) under different comparisons (*Unpredicted Local*, *Predicted Local*, or *Global*) and conditions (*Full-global*, *Partial-global*, or *No-global*). "*" indicates that the prediction-error signal appears in the corresponding comparison, and "--" indicates that the error signal cannot be detected by the corresponding comparison.

(AAAAB or BBBBA, jointly denoted by xxxxY). Auditory stimuli were delivered in blocks of 120 trials within which one auditory sequence was frequent while another was rare. In xxxxx blocks, 20 xxxxx trials were initially delivered to establish the rule; then, there was a random mixture of 80 xxxxx trials (denoted by $xx|xx$: xxxxx trial in xxxxx block) randomly mixed with 20 trials of the deviant sequence xxxxY ($xY|xx$: xxxxY trial in xxxxx block). Conversely, in xxxxY block, 20 trials of xxxxY were initially delivered, followed by a random mixture of 80 xxxxY trials ($xY|xY$: xxxxY trial in xxxxY block) and 20 xxxxx trials ($xx|xY$: xxxxx trial in xxxxY block).

This paradigm was designed to contrast two levels of regularity. A local regularity is established within a trial by the repetition of the first 4 tones, which is either followed or violated by the fifth tone. A global regularity is established by habituating the subject

to a specific 5-tone sequence, which is either respected or violated by subsequent sequences. Local and global regularities are orthogonally varied, yielding four trials types: local and global standards ($xx|xx$), local and global deviants ($xY|xx$), local deviant but global standard ($xY|xY$), and local standard but global deviant ($xx|xY$).

A Hierarchical Predictive-Coding Model of Local and Global Novelty

The predictive-coding theory suggests that the brain generates predictions about the possible incoming sensory events, and that the difference between the prediction and actual sensory input, i.e., prediction error, propagates forward throughout the cortical hierarchy. Figure 2 shows how the predictive-coding framework may provide qualitative predictions about neural

responses in the local-global paradigm. We hypothesize a model with two hierarchical levels of predictions and prediction errors interacting in two neuronal populations: one for processing the local standard tone x , and the other for processing the local deviant tone Y . The lower-level system predicts tones solely based on their transition probabilities (Meyniel et al., 2016); the higher-level system uses the learned sequence to predict error signals from the lower level when local deviants are expected by the global rule, and thus to reduce or abolish the propagation of those error signals up to a higher level.

This model predicts that a two-step propagation of error signals should be observed in $xxxx$ blocks (Figure 2A). On $xx|xx$ trials, the fifth tone x should be predicted by the lower-level prediction ($P1x$), and thus no prediction error should be generated. On $xY|xx$ trials, error signals should occur at the lower level since the expected tone x is omitted ($PE1x$) and the observed tone Y is unpredicted ($PE1Y$). Such unexpected violations should continue to propagate to the next hierarchical level ($PE2x$ and $PE2Y$). On the other hand, the effects of higher-level predictions should be specifically observed in $xxxxY$ blocks (Figure 2B). First, on $xY|xY$ trials, a lower-level prediction error should still occur, since the final tone Y violates the transition probability established by the previous stream of $xxxx$. But because this local violation is now expected by the higher-level predictions ($P2x$ and $P2Y$), its propagation to the higher-level should be completely canceled out if the global regularity is fully learned (*Full-global*), or be reduced if the global regularity is only partially learned (*Partial-global*). If the global regularity is completely unlearned (*No-global*), the local violation should continue to propagate as on $xY|xx$ trials. Second, on $xx|xY$ trials, only a higher-order violation should be observed, caused by the unexpected absence of an expected local violation.

The model further predicts that different hierarchical processes can be isolated by comparing brain activity evoked by different stimuli (Figure 2C). By contrasting $xY|xx$ and $xx|xx$ trials, we can isolate novelty responses that arise when both local and global regularities are violated, i.e., a local novelty response that is also unpredicted by the global rule (unpredicted local novelty response, or *Unpredicted Local*). Similarly, by contrasting $xY|xY$ and $xx|xY$ trials, we can capture the local novelty response that is predicted by the global rule (predicted local novelty response, or *Predicted Local*). Finally, by contrasting rare trials (*Rare*, includes $xY|xx$ and $xx|xY$) and frequent trials (*Frequent*, includes $xx|xx$ and $xY|xY$), we can isolate the global novelty response (global novelty response, or *Global*). Based on the model (as in Figures 2A and 2B), lower-level prediction-error signals ($PE1$, includes $PE1x$ and $PE1Y$) should appear in the unpredicted and predicted local novelty responses but not in the global novelty response, and higher-level prediction-error signals ($PE2$, includes $PE2x$ and $PE2Y$) should appear in all novelty responses (in *Full-global*), only in the unpredicted local and global novelty responses (in *Partial-global*), or only in the unpredicted and predicted local novelty responses (in *No-global*). It is worth noting that the term “novelty” is used here to describe responses to sequences that violate the rule, even though the sequences themselves are not novel since they occur multiple times in a block.

Three Novelty Response Patterns Revealed by Univariate Analysis

To test the model predictions, we compared ECoG signals from different trial conditions to obtain novelty responses from the three comparisons: unpredicted local novelty response ($xY|xx - xx|xx$), predicted local novelty response ($xY|xY - xx|xY$), and global novelty response (*Rare - Frequent*). The spatio-spectro-temporal dynamics of ECoG signals were quantified by the time-frequency representation (TFR) obtained from wavelet transformation. Each TFR represents the in-trial cortical dynamics from a channel, during the time from 200 ms before the first tone to 600 ms after the fifth tone (81 time bins), across the frequencies between 0 and 125 Hz (125 frequency bins).

An example of the three comparisons of TFRs in channel 78, located in early auditory cortex (rostral parabelt area), is shown in Figure 3. A novelty response was defined as a significant difference in TFRs under the corresponding comparison (contoured areas in Figure 3), detected by a nonparametric cluster-based permutation test ($\alpha = 0.05$ corrected for multiple comparisons, see STAR Methods). In the predicted local novelty response (middle row in Figures 3), an early γ -band power increase (>40 Hz) appeared right after the fifth tone. In the unpredicted local and global novelty responses (top and bottom rows, respectively), the γ -band power increase appeared not only in the early phase, but also extended to a later phase, where the early and late γ -band power increases jointly lasted more than 300 ms. Other than the γ -band power increases, the unpredicted local novelty response also contained a β -band power decrease (10~30 Hz) with a longer latency (top row).

These spectro-temporal patterns (the early γ -band increase, late γ -band increase, and late β -band decrease) were also observed in other channels in both subjects (see novelty responses from all 128 channels in both subjects in Figure S1). A simple univariate analysis was used to identify the patterns across all channels (Figure 4A). Most responses were found at the temporal and frontal sites, and, in subject 1, the orbitofrontal cortex (OFC) and each spectro-temporal pattern showed distinct spatial distribution. To see how each response pattern contributed to different novelty responses, we counted the total number of channels that contained the response pattern (Figure 4B). In both subjects, the early γ -band increase appeared more in the unpredicted and predicted local novelty responses than in the global novelty response, which closely matched the expected appearance profile of $PE1$ (Figure 2C). On the other hand, the late γ -band increase and β -band decrease were primarily found in the unpredicted local and global novelty responses, which matched the expected appearance profile of $PE2$ in the *Partial-global* model (Figure 2C). Moreover, the late γ -band increase and β -band decrease could represent opposite hierarchical signaling in the processing of $PE2$, since the γ and β bands are thought to subserve bottom-up and top-down communications, respectively (see Discussion).

In summary, our initial univariate analysis suggested that (1) the early γ -band power increase represented a bottom-up $PE1$ processing, (2) the late γ -band power increase represented a subsequent bottom-up $PE2$ processing, (3) the late β -band power decrease represented a top-down modulation process

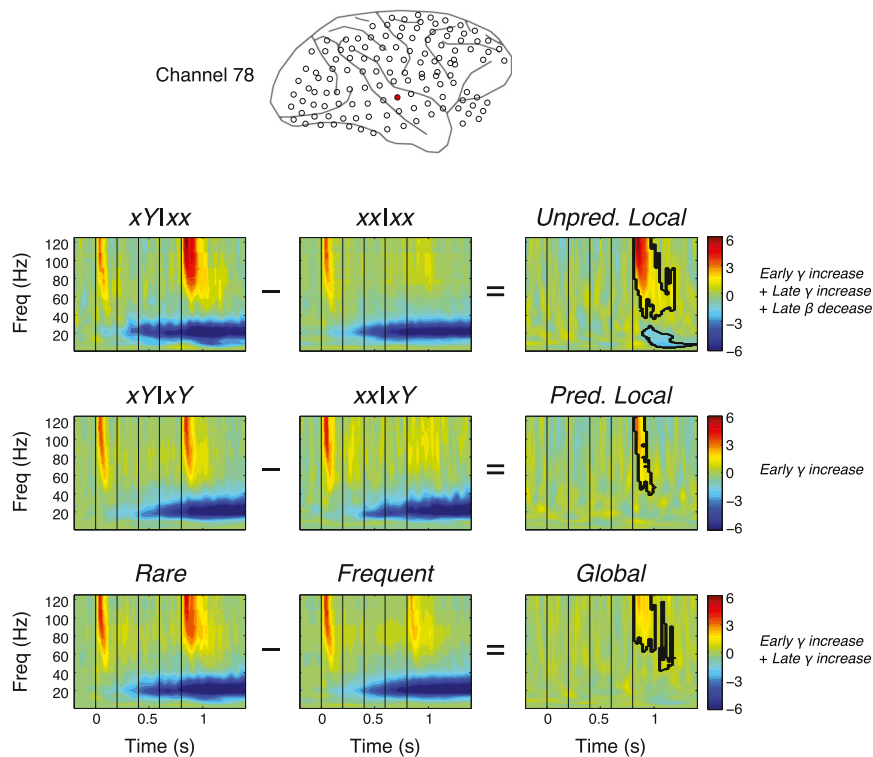


Figure 3. Examples of Partially Superimposed Local and Global Novelty Responses
Comparisons of TFRs in channel 78 (red circle). Averaged TFRs in different trial types are shown (first two columns), and the significant differences between them, i.e., novelty responses, are outlined (third column). The vertical lines indicate the five stimuli on each trial. The color represents the relative activation level, measured in decibel, compared to the baseline values (−0.2–0 s).

associated with *PE2*, and (4) the global regularity was only partially predicted (*Partial-global* in Figure 2).

Three Latent Components in Comprehensive Dynamics of Network Activity Identified by Data-Driven Analysis

To further test the hypotheses suggested by the univariate analysis, we aimed to acquire a more comprehensive view of the novelty responses across the large space of channels, time, frequencies, and conditions. This was achieved by using an unbiased decomposition analysis that extracts latent components in functional network dynamics (Chao et al., 2015) (see *STAR Methods* and Figure S2). We first pooled novelty responses from all channels and all comparisons to create a broadband library. To organize and visualize this dataset, we created a tensor with three dimensions: *Channel* (cortical area), *Time-Frequency* (in-trial dynamics), and *Comparison* (novelty response), for the anatomical, dynamic, and functional aspects of the data, respectively. The dimensionality of the tensor was 128 (channels) by 10,125 (125 time windows and 81 frequency bins) by 3 (comparisons). To extract structured information from the dataset, we factorized the 3D tensor into multiple components by performing parallel factor analysis (PARAFAC), a generalization of principal-component analysis (PCA) to higher-order arrays (Harshman and Lundy, 1994) and measured the consistency of factorization under different iterations of PARAFAC (Bro and Kiers, 2003) (see *STAR Methods*).

Three dominant components were identified from the pooled activity (Figure S3), where each component contained a unique fingerprint of network anatomy, dynamics, and function, described by its composition in the three tensor dimensions (Figure 5). The three components matched the three response

patterns found in the initial univariate analysis. For subject 1, component 1 was associated with the early γ -band power increase. It was activated mainly in early auditory cortex (particularly the rostral parabelt area) (Figure 5A, top), immediately after the fifth tone and in the γ frequency band (>40 Hz) (Figure 5B, top) (see the temporal and spectral profiles in Figure S4). Furthermore, it appeared mostly in the unpredicted and predicted local novelty responses (Figure 5C, top). Component 2 was associated with the late γ -band power increase. It was activated primarily in the anterior temporal cortex (particularly areas Ts1 and Ts2 in the superior temporal gyrus) and secondarily in PFC (particularly the frontopolar area 10) and the OFC (Figure 5A, middle), slightly after component 1 but also in the γ frequency band (Figure 5B, middle), and appeared mostly in the unpredicted local and global novelty responses (Figure 5C, middle). Component 3 was associated with the late β -band power decrease. It was activated primarily in PFC (particularly the frontopolar area 10) and secondarily in the superior temporal cortex and OFC (Figure 5A, bottom), slightly after component 2 and with a decrease in α/β -band power (<30 Hz) (Figure 5B, bottom), and appeared mostly in the unpredicted local and global novelty responses as in component 2 (Figure 5C, bottom). Remarkably similar components were found in subject 2, except the strong activations in PFC were found in the dorsolateral PFC (DLPFC), and OFC was not recorded (Figures 5D–5F).

The data-driven results supported our hypothesis in all three dimensions. Anatomically (Figures 5A and 5D), component 1 was located around early auditory cortex, in agreement with its role in the processing of local prediction error, and components 2 and 3 were located in higher-order cortices, in agreement with roles in higher-order sequence-level processing. Dynamically (Figures 5B and 5E), the activation timings and spectral profiles indicated that a bottom-up process (component 1) was activated right after the fifth tone, followed by another bottom-up process (component 2) and a subsequent top-down process (component 3). Functionally (Figures 5C and 5F), the components' contributions to the novelty responses were consistent with the *Partial-global* model (Figure 2C) and the results from the univariate analysis (Figure 4B),

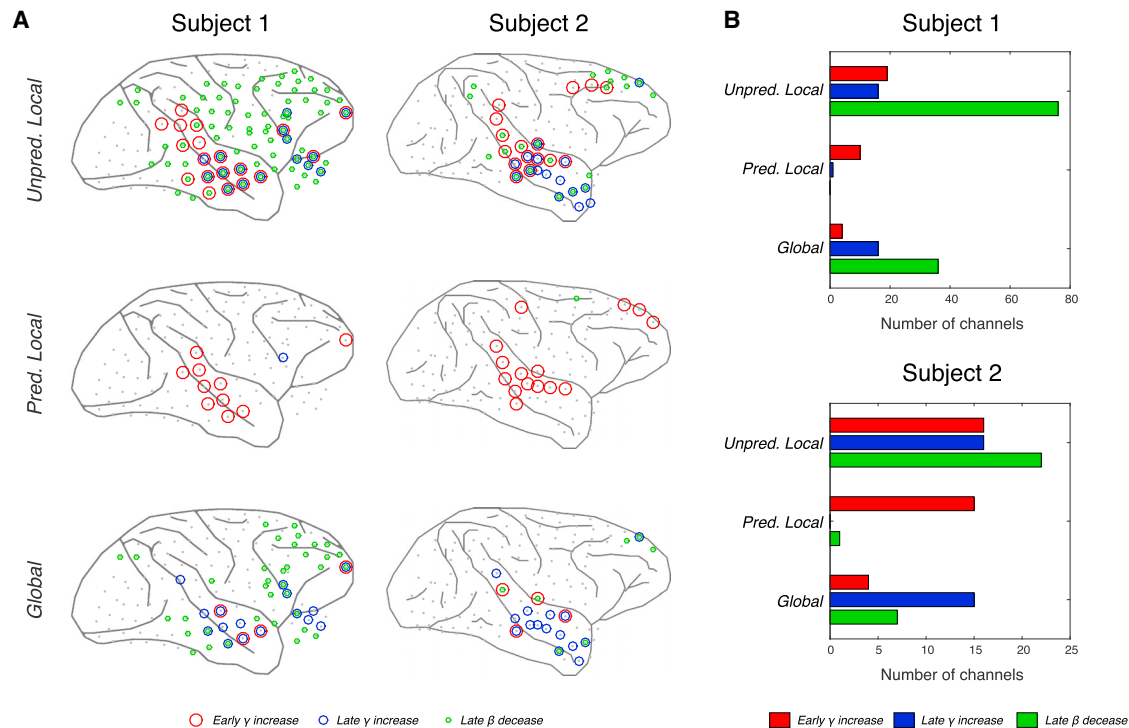


Figure 4. Spatial Distribution of Different Novelty Response Patterns

(A) The channels contained early γ -band power increases (red circles), late γ -band power increases (blue), and/or late β -band power decreases (green) in novelty responses (top: the unpredicted local novelty response, middle: the predicted local novelty response; bottom: the global novelty response) are shown for subjects 1 (left) and 2 (right). Gray dots indicate the locations of all 128 channels.

(B) The number of channels shown early γ -band power increases (red), late γ -band power increases (blue), and/or late β -band power decreases (green) in different novelty responses are shown for subjects 1 (top) and 2 (bottom). The spectro-temporal patterns of all novelty responses are shown in Figure S1.

again suggesting that component 1 represented the processing of *PE1*, and components 2 and 3 were related to the processing of *PE2*.

Component 3 as a Top-Down Process Tested by Directional Network Connectivity

Our results consistently linked components 1 and 2 to *PE1* and *PE2*, respectively, while component 3 as a top-down process was so far a speculation based on its frequency characteristics. To verify that component 3 indeed indexed a top-down process, we examined the directionality of corticocortical interactions in the novelty responses. Corticocortical interactions were quantified by spectral Granger causality (GC) (see STAR Methods), which uses the phase differences between signals from two cortical areas to infer their asymmetric causal dependence (Brovelli et al., 2004; Kamiński et al., 2001). Each GC represents the in-trial spectro-temporal dynamics of corticocortical interactions for a given pair of electrodes, during the time from 200 ms before the first tone to 600 ms after the fifth tone (81 time bins), and across frequencies between 0 and 125 Hz (125 frequency bins).

Similar to the activity analysis on TFRs, we compared GCs across different trial conditions in order to examine changes in connectivity induced by novelty stimuli. We then pooled novelty connectivity responses from all connections and all comparisons to create a tensor with three dimensions: *Channel-Channel*

(cortical connection), *Time-Frequency* (in-trial dynamics), and *Comparison* (novelty response). For each subject, the dimensionality of the tensor was 16,256 (connections) by 10,125 (125 time windows and 81 frequency bins) by 3 (comparisons). We then factorized the 3D connectivity tensor by performing PARAFAC, and only one principal component from the pooled connectivity was identified (Figure S5).

For both subjects, the principal connectivity component involved connections from PFC to the temporal cortex (Figure 6A), about 200 ms after the fifth tone and in the α and β frequency bands (<30 Hz) (Figure 6B), and appeared only in the unpredicted local and global novelty responses (Figure 6C). To further visualize the connectivity patterns, we quantified the causal density and causal outflow of the interactions (Figure 6D). Causal density is the sum of all outgoing and incoming interactions for each channel, showing areas with busy interactions. Causal outflow is the net outgoing interactions of each channel, indicating the source and sink areas of interactions. Busy interactions were found in the connections from DLPFC to early auditory cortex, anterior temporal cortex, and OFC (in subject 1).

The principal connectivity component could represent the same process as component 3, since they shared similar anatomical, dynamic, and functional profiles. Spatially, both involved PFC, early auditory cortex, anterior temporal cortex, and OFC (in subject 1); spectrally, both appeared in the lower-frequency

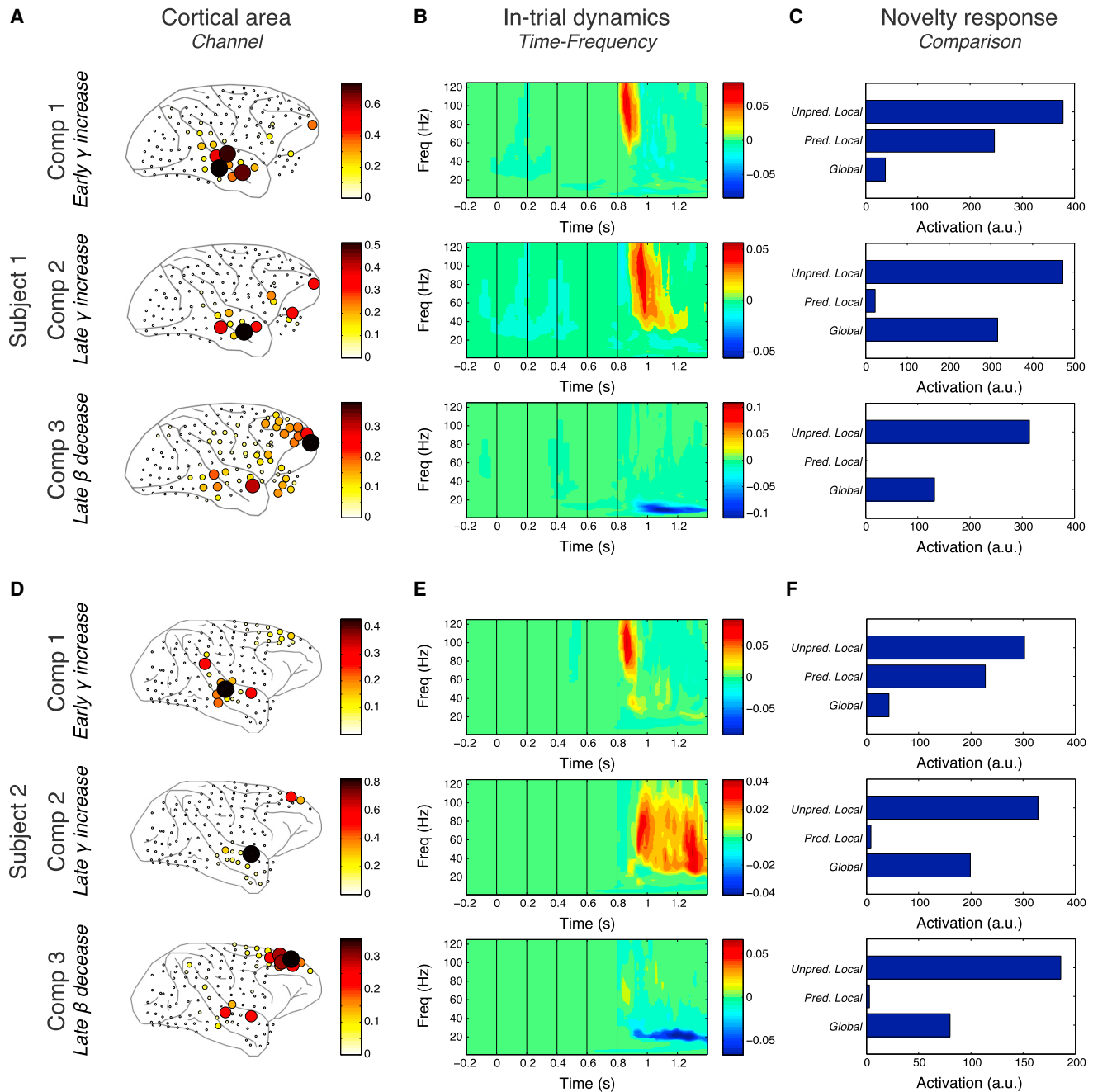


Figure 5. Principal Activity Components in Novelty Responses

(A) The anatomical dimension of the three components in subject 1. The size and color of each circle represent the activation level (arbitrary unit) at the corresponding electrode.

(B) The dynamic dimension of the three components in subject 1.

(C) The functional dimension of the three components in subject 1.

(D–F) The same as (A)–(C), but the results are from subject 2.

bands (<30 Hz); and, functionally, both were absent from the predicted local novelty response. Therefore, component 3 could be indeed associated with top-down information flow triggered by *PE2*, compatible with a role in updating predictions and resolving errors arising in the lower-level auditory cortices.

Coordination among Activity Components Tested by Within-Trial Functional Correlations

To further verify the postulated roles of the three components, we examined their coordination by evaluating how their activations co-varied with each other within individual trials under

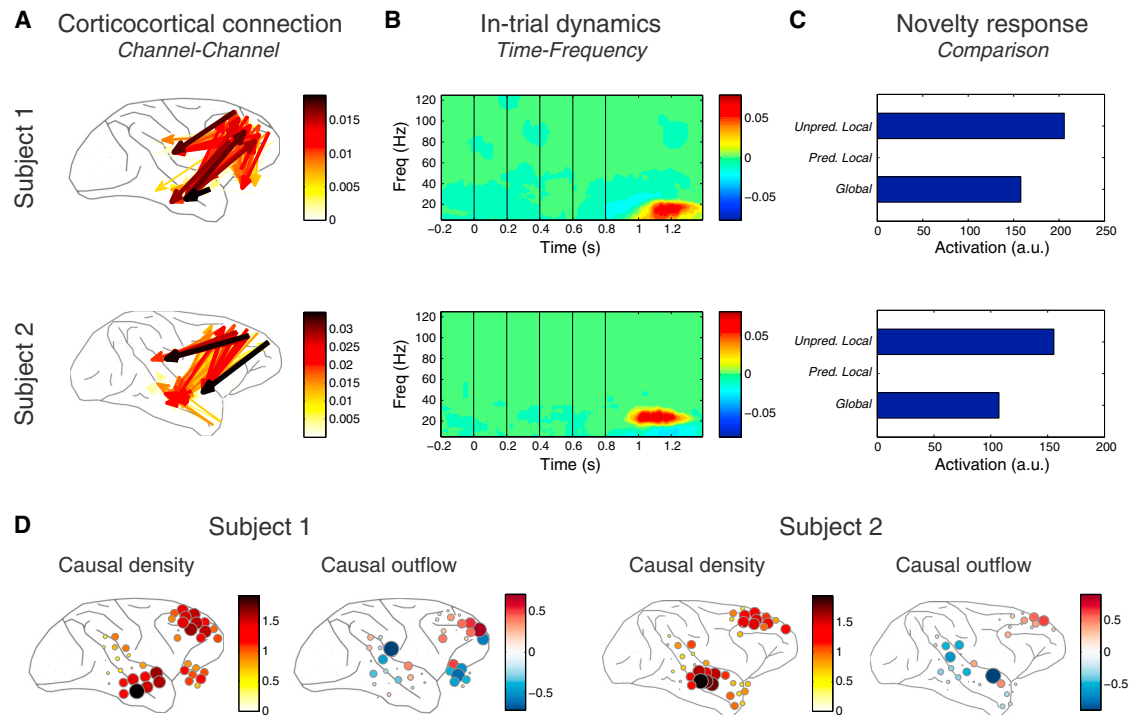


Figure 6. Principal Connectivity Component

(A) The anatomical dimension of the principal connectivity component in subjects 1 (top) and 2 (bottom). The width and color of each arrow represent the activation level (arbitrary unit) in the corresponding connection.
 (B) The dynamic dimension of the connectivity component.
 (C) The functional dimension of the connectivity component.
 (D) Causal density and causal outflow of the connectivity component in subject 1 (left) and 2 (right). For causal density, the size and color of each circle represent the sum of all outgoing and incoming interactions at the corresponding channel. For causal outflow, the size and color of each circle represent the net outgoing interactions of each channel, where red and blue channels represent source and sink areas of the information flow, respectively.

different trial conditions. The predictive-coding model predicts that the activation level of component 1 (*PE1*) should determine the activation level of component 2 (*PE2*), especially on $xY|xx$ trials, which is consistent with the model where no prediction error arises on $xx|xx$ trials. Second, significant correlations between components 1 and 2 were found on $xY|xx$ and $xY|xY$ trials, which is consistent with the model where *PE2* (component 2) was causally induced by *PE1* (component 1) on $xY|xx$ and $xY|xY$ trials. Lastly, significant correlations were found between components 2 and 3 on $xY|xx$, $xY|xY$, and $xx|xY$ trials, which suggested that *PE2* always led to a top-down prediction update (component 3). Furthermore, the correlations were stronger on $xY|xx$ trials than on $xY|xY$ and $xx|xY$ trials, as predicted by the model.

To evaluate these hypotheses, we first estimated how much each multidimensional component contributed to individual trials. This was achieved by projecting the TFR of each trial onto the spatio-spectro-temporal pattern (the first two dimensions) of each component (see [STAR Methods](#)). As result, how much each component contributed to the novelty response on a given trial was represented by a single scalar, i.e., its projection value. Examples of contributions of the three components during $xx|xx$ and $xY|xx$ trials are shown in [Figure S6](#). We then evaluated whether the contribution of one component correlated with the contribution of another component (full statistics in [Table S1](#)). Significant correlations under all trial conditions in both subjects are illustrated in [Figure 7A](#).

The functional correlations strongly supported the proposed predictive-coding model. First, no correlation was found on $xx|xx$ trials, which is consistent with the model where no prediction error arises on $xx|xx$ trials. Second, significant correlations between components 1 and 2 were found on $xY|xx$ and $xY|xY$ trials, which is consistent with the model where *PE2* (component 2) was causally induced by *PE1* (component 1) on $xY|xx$ and $xY|xY$ trials. Lastly, significant correlations were found between components 2 and 3 on $xY|xx$, $xY|xY$, and $xx|xY$ trials, which suggested that *PE2* always led to a top-down prediction update (component 3). Furthermore, the correlations were stronger on $xY|xx$ trials than on $xY|xY$ and $xx|xY$ trials, as predicted by the model.

Component 3 as Prediction Updates Tested by Across-Trial Functional Correlations

We demonstrated that component 3 represented a top-down process that was triggered by the higher-level error *PE2*. Our hypothesis is that component 3 represents a prediction update process that resolved prediction errors at the same hierarchical level (*PE2*) and/or at the lower level (*PE1*). One final prediction is that this model update would affect the processing of subsequent trials. Specifically, trial-by-trial fluctuations in the strength of activation of component 3 should affect the amount

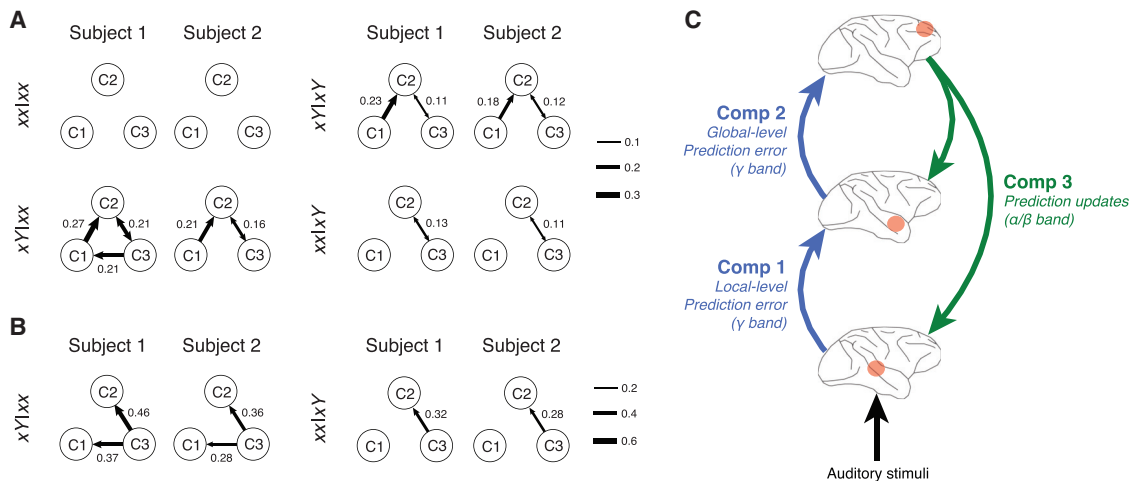


Figure 7. Evaluation of Functional Correlations between Activity Components within and across Trials

(A) Illustration of the functional correlations between the components within a trial in different trial types. Each black line indicates a significant correlation ($p < 0.05$), and the corresponding correlation coefficient is labeled and represented by its thickness. The direction of each arrow indicates the temporal order of the components, not their functional causality. See full statistics in [Table S1](#).

(B) Illustration of the functional correlations between component 3 on the global deviant trials (left: $xY|xx$: global deviants in $xxxxx$ block; right: $xx|xY$: global deviants in $xxxxY$ block) and components 1 and 2 on the following standard trials (post-deviant). Each black line indicates a significant correlation ($p < 0.05$), and the corresponding correlation coefficient is labeled and represented by its thickness. The direction of each arrow indicates the temporal order of the components, not their functional causality. See full statistics in [Table S2](#).

(C) Schematics of the proposed hierarchy of cortical signals coding for $PE1$ (component 1), $PE2$ (component 2), and prediction updates (component 3) and their corresponding cortical areas and frequency channels.

of changes in top-down predictions and affect prediction-error signals on subsequent trials. We therefore predicted that the activation level of component 3, on a global deviant trial, should determine the activation levels on component 2 ($PE2$) and/or component 1 ($PE1$) on the next trial (which is always a global standard).

Similar to the previous analysis, each single-trial response was first projected to the three components to capture each component's contribution. We then evaluated whether the contribution of component 3 on the global deviant trials, in both $xxxxx$ block (i.e., $xY|xx$ trials) and $xxxxY$ block (i.e., $xx|xY$ trials), was correlated to the contributions of components 1 and 2 on the corresponding post-deviant trials. Examples of each component's contribution in $xxxxx$ block are shown in [Figure S7](#).

The correlations were observed as predicted by the hierarchical predictive-coding model (full statistics in [Table S2](#)). Particularly, the activation level of component 3 on $xY|xx$ trials was significantly correlated to the post-deviant activation levels of components 1 and 2, and the activation level of component 3 on $xx|xY$ trials was significantly correlated to the post-deviant activation level of component 2 ([Figure 7B](#)). These results indicated that when both local and global regularities were violated (as on $xY|xx$ trials, [Figure 2A](#)), component 3 influenced both $PE1$ and $PE2$ on the next trial. On the other hand, when only global regularity was violated (as on $xx|xY$ trials, [Figure 2B](#)), component 3 influenced only $PE2$ on the next trial.

Extraction of Partial Global Prediction Signals

The results from our analyses all supported the model of partial global prediction (*Partial-global*). To further examine how the

prediction of global regularity was established, we switched our focus to the first 20 repetitive $xxxxY$ trials in $xxxxY$ blocks. We hypothesized that the global prediction was absent or weak in the early trials and gradually established over the repetitions. Therefore, neural processes during the early trials should be similar to $xY|xY$ in *No-global*, and neural processes during the later trials should be similar to $xY|xY$ in either *Full-global* or *Partial-global* ([Figure 2B](#)).

To extract the global prediction signals, we therefore compared the TFRs from the first 3 trials (*Early*, trials 1–3) to the TFRs from the last 3 trials (*Late*, trials 18–20). The significant difference in TFRs between *Early* and *Late* trials (*Late – Early*) was detected by the same nonparametric cluster-based permutation test used in [Figure 3](#) ($\alpha = 0.05$ corrected for multiple comparisons). All the identified significant differences are shown in [Figure 8](#). In subject 1, the significant differences were found primarily in DLPFC and the frontopolar area 10, secondarily in the dorsal premotor cortex (PMd) (particularly the premotor area F2), and also the area Ts2 in the superior temporal gyrus ([Figure 8A](#), left). In subject 2, the significant differences were found primarily in DLPFC, and secondarily in PMd (the area F2) and the ventral premotor cortex (PMv) (the area F5) ([Figure 8A](#), right). In both subjects, the significant differences were found in the α/β -band power (<30 Hz) as early as the end of the first tone ([Figure 8B](#)).

Based on the model in [Figure 2](#), if the global prediction was fully established in *Late* trials, the significant difference (*Late – Early*) should contain not only the higher-level predictions ($P2x$ and $P2Y$, present in *Late* trials), but also the higher-level prediction errors ($PE2x$ and $PE2Y$, present in *Early* trials) (compare

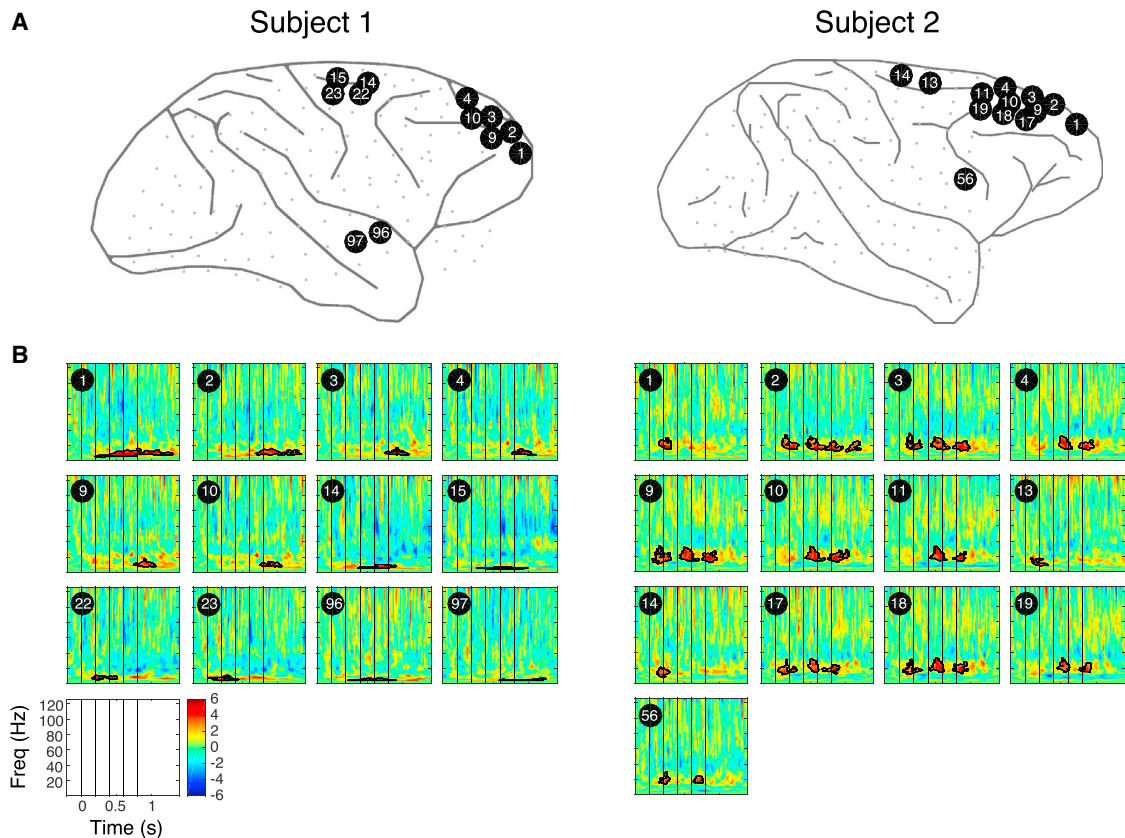


Figure 8. Emergence of Global Prediction Signals within the First 20 Trials of a Block

(A) Channels with a significant difference in TFRs between *Early* and *Late* trials ($Late - Early$) are shown with large black circles with the channel numbers labeled. Non-significant channels are indicated by small gray dots.

(B) Time-frequency representations of the identified significant differences. Each panel represents a significant channel shown in (A) (the channel number is shown). Same format as Figure 3. Axis labels and color bar are shown in the lower-left corner.

$xY|xY$ in *Full-global* and *No-global*). On the other hand, if the global prediction was only partially established, where the higher-level prediction errors also appear in *Late* trials, the significant difference should primarily reflect the higher-level predictions (compare $xY|xY$ in *Partial-global* and *No-global*). Since the higher-level prediction error should appear in the γ band and no significant γ -band responses were observed (Figure 8B), we concluded that, during the emergence of the rule in the first 20 trials of a block, brain activity was dominated by the establishment of a partial prediction for the global regularity.

We further performed a similar comparison between the first 3 $xxxxY$ trials after the 20 repetitions (around trials 21–23, $xxxxx$ trials were skipped) and the 3 $xxxxY$ trials after a comparable 20-trial period (around trials 38–40, $xxxxx$ trials were skipped). Most of the prediction signals identified in the first 20 trials was not found in the following 20 trials (Figure S8). This indicated that the identified prediction signals were not an artifact of drift in neural activity, and the learning of global regularity occurred primarily during the first 20 repetitions. Furthermore, it is worth noting that our task only required the subjects to passively listen to the stimuli and thus provided no behavioral assessment for this internal learning process.

DISCUSSION

To evaluate the hierarchical predictive-coding model during the local-global paradigm, we used a data-driven approach to extract emergent network components in cortical activity and cortico-cortical connectivity, which were further tested by hypothesis-driven analyses. Our findings revealed the presence of three distinct cortical processing stages for auditory novelty and determined their functional correlations and hierarchy (summarized in Figure 7C). Based on our results, we proposed that prediction-error signals are transmitted in the γ frequency band, where the local-level prediction-error signal is sent from early auditory cortex to the anterior temporal cortex, and the global-level prediction-error signal is sent from the anterior temporal cortex to PFC. On the other hand, the local- and global-level prediction signals are transmitted in the α/β band, between the same corresponding areas but in the opposite directions. Furthermore, if a local-level prediction error is not fully cancelled out by the global-level prediction, then a prediction-update signal is triggered in the α/β band and broadcasted from PFC back to the anterior temporal cortex and early auditory cortex, which are the target areas of the global- and local-level prediction signals, respectively.

Significance of the Hierarchical Structure

According to the hierarchical predictive-coding framework (Friston, 2005), higher levels of the cortical hierarchy predict the error residual from the lower level rather than the sensory data itself. Another possible model is a predictive but not hierarchical design, where one top-down process predicts the local regularity, as in the hierarchical model, and the other process directly predicts the global regularity in the input sequence. According to this alternative non-hierarchical model, the top-down process should directly predict the fifth tone x in $xxxx$ block and the fifth tone Y in $xxxxY$ block; therefore, the novelty response in $xxxx$ block ($xY|xx - xx|xx$) should be equivalent to the novelty response in $xxxxY$ block ($xx|xY - xY|xY$). However, this is disproved by our results, which showed that $xY|xx - xx|xx$ (the unpredicted local novelty response) and $xx|xY - xY|xY$ (the negative of the predicted local novelty response) contained different components and were always different. The key advantage of having hierarchies in a bidirectional structure is to allow information related to regularities at different spatial and temporal scales to merge into a coherent unity, because each hypothesis about the hidden causes of sensory inputs is called upon only if the sensory data cannot be explained at a lower level; such a hierarchical organization may therefore result in an internally consistent model of the causal structure of the sensory world (Clark, 2013; Friston, 2010).

Dissecting Complex Multi-Dimensional Brain Responses

Neurophysiological responses can be dissected into at least four dimensions: anatomical site, temporal dynamics, frequency selectivity, and stimulus responsivity. Here, we show how a comprehensive description of such complex brain responses, indexing neural processes that are multi-dimensional, simultaneous, and interdependent, can be achieved by using the PARAFAC method of tensor decomposition. PARAFAC is one of several methods to decompose a multi-dimensional data into a set of latent components that can describe the data in a more condensed form. Other commonly used methods are the Tucker3 method (Kroonenberg, 1983) and simply unfolding of the multi-dimensional data to a 2D matrix and then performing standard two-way methods such as PCA. Among these methods, PARAFAC uses fewer degrees of freedom to model the data (Kiers, 1991) and does not require matrix unfolding, which will mix up the variables and destroy their interactions (Harshman and Lundy, 1994). Those features make PARAFAC simpler, more robust, and ideal to extract latent patterns in the data for easier interpretation. PARAFAC has proved to be a powerful analytical tool for electroencephalography (EEG) (Miwakeichi et al., 2004; Mørup et al., 2006), ECoG (Chao et al., 2015; Yanagawa et al., 2013), and fMRI (Beckmann and Smith, 2005) and is well suited to dissect brain responses that consist of multiple superimposed network dynamics (Chao et al., 2015, 2018).

Brain Areas Associated with Local and Global Novelty

Our result shows that lower- and higher-order auditory prediction errors are represented in the temporal and frontal cortices, respectively. This is consistent with previous evidence from

both monkey and human studies using the local-global paradigm or its variations. Human studies with ECoG, EEG, MEG, and fMRI show that local error signals are confined to the primary auditory cortex, while global error signals propagate to distributed areas in the frontal cortex (Bekinschtein et al., 2009; Chennu et al., 2013; El Karoui et al., 2014; Wacongne et al., 2011). Similar results have been found in monkeys, where fMRI responses to local and global violations are identified in the auditory cortex and a distributed frontoparietal network, respectively (Uhrig et al., 2014). In the framework of predictive coding, temporal cortex has been suggested to be involved in the learning and storing of transition probabilities, which suffice to detect local deviants (Wacongne et al., 2011). Frontal cortex, on the other hand, was found to encode more global and abstract properties of the entire sequence, including numerical patterns (“there should be 5 items”) and sequential patterns (“the last item should be different”) in both monkeys and humans (Wang et al., 2015), compatible with its present activation to global deviants.

In our study, the higher-order error and update signals were found primarily in the frontopolar PFC (area 10) and DLPFC. Among prefrontal areas in macaque monkeys, the frontopolar area 10 has the densest interconnection with auditory association areas: it receives information from nearly all levels of auditory processing in the superior temporal gyrus, from the early sensory processing in the belt and parabelt areas to the higher-order processing of conspecific communication in the temporal polar areas (Medalla and Barbas, 2014; Romanski and Averbeck, 2009) and is also the main source of connections back to auditory cortices (Barbas et al., 2005). Functionally, both the frontopolar area 10 and DLPFC are important for working memory (Curtis and D’Esposito, 2003; Gilbert et al., 2006). The present results suggest that those brain structures generate and hold an internal representation of the entire sequence of stimuli, sufficient to generate error signals when an unexpected sequence is heard.

The ventrolateral PFC (VLPFC) is another key area for processing auditory sequences, particularly those with higher complexity (Wilson et al., 2017). Previous studies with the local-global paradigm have shown that global novelty responses can be found in VLPFC in both monkeys and humans (Uhrig et al., 2014; Wang et al., 2015). In agreement with those findings, our univariate analysis identified several electrodes in VLPFC in subject 1 that showed late γ -band power increases and β -band power decreases in the global novelty response (Figure 4A), although the responses were smaller than those in the frontopolar area 10 and DLPFC (Figure 5A). In subject 2, unfortunately, the role of VLPFC could not be evaluated since electrode placement failed to cover the area (Figure 1B). In contrast to the frontopolar cortex and DLPFC, which showed signals associated with both the global prediction (Figure 8) and its updates, VLPFC was only found involved in the update process. This suggested a distinctive modulatory role of VLPFC in auditory sequence encoding and storage. Further research, using recordings specifically focused on this region and using a greater variety of auditory sequences will be needed to evaluate the hypothesis that inferior frontal cortex acts as a conserved sequence processor in humans and monkeys (Wilson et al., 2017), and the possibility that its representational scheme has expanded in human evolution (Dehaene et al., 2015).

Brain Signals and Areas Associated with Global Prediction

Analysis of the evolution of brain signals during the first 20 trials in a block showed how the partial global prediction signals built up during the repetitions of xxxxY. Using this approach, we found that global prediction signals appeared as early as the end of the first tone in the sequence (Figure 8B). This result suggests that global prediction is not based on a static pattern of neural activity that would be maintained throughout the xxxxY block, but on a dynamic, trial-specific signal. Global prediction signals could have been launched by an attention engagement triggered by the fixation onset, which occurred 200–300 ms before the first tone (see STAR Methods and Figure 1A). Alternatively, global prediction signals could have been directly triggered by the first tone, suggesting the existence of another bottom-up pathway that launched the global prediction from the onset of a sensory sequence.

Global prediction signals were found primarily in PFC and the premotor cortex (Figure 8A). Among those areas, DLPFC and the frontopolar area 10 were also involved in the processing of higher-order errors and prediction updates (Figures 5A and 6B). This finding suggests that PFC was the core structure maintaining an internal representation of the entire xxxxY sequence and could receive global-level prediction-error signals from the lower hierarchy and send prediction-update signals to the lower hierarchies when the global deviant occurred (xxxxx). On the other hand, the premotor cortex was found to be activated in humans during the monitoring of auditory violations in a serial prediction task (Schubotz et al., 2003), predicting musical rhythms (Chen et al., 2008; Chen et al., 2006; Zatorre et al., 2007), and speech perception (Meister et al., 2007; Pulvermüller and Fadiga, 2010). The identified involvement of the premotor cortex supports the view that sound and action are often intrinsically linked (the sounds we hear reflect actions, and the sounds we make result from actions), and that motor signals are therefore involved in the prediction of sensory events (Lima et al., 2016; Morillon and Baillet, 2017; Schubotz, 2007).

Gamma and Alpha/Beta Oscillations in Predictive Coding

Neural oscillations are thought to be a means for neuronal populations to communicate within and between cortical areas, where different frequency channels are associated with different types of neural computations (Fries, 2005). This notion is supported by recent studies of the human and primate cortex, which have shown that feedforward and feedback hierarchical communication between cortical areas are exerted through γ - and α/β -band oscillations, respectively, in both vision (Bastos et al., 2015b; Michalareas et al., 2016; van Kerkoerle et al., 2014) and audition (Dürschmid et al., 2016; Fontolan et al., 2014; Sedley et al., 2016). In the present study, we examined this view in the context of predictive coding and demonstrated that ascending information about prediction errors and descending information about predictions and prediction updates were indeed processed in the γ and α/β frequency bands, respectively. This finding suggests the significance of directional frequency-specific multiplexing in cortical information processing.

Numerous human ECoG and MEG studies have demonstrated the correlation between prediction errors and the magnitude of γ -band oscillations in audition (Dürschmid et al., 2016; Edwards et al., 2005; Todorovic et al., 2011), vision (Brodzki et al., 2015), and audiovisual interactions (Arnal et al., 2011). To further examine the hierarchical structure in prediction errors, a human ECoG study with the local-global paradigm shows that local novelty evokes early high- γ responses (60~120 Hz) in the temporal cortex, whereas global novelty induces a sustained decrease in the β -band power (13–25 Hz) within the frontal lobe (El Karoui et al., 2014). With the same paradigm, we obtained similar results in monkeys. However, we found that prediction errors at the local and global levels are both represented in the γ oscillations, but with slightly different frequency profiles (Figure S4). This “frequency ordering” suggests that bottom-up error signals could be carried by slightly different frequency channels depending on their level in the hierarchy. Furthermore, we found that the β -power decrease in the global novelty response is not associated with prediction errors, but with a top-down prediction update.

Although their role in top-down versus bottom-up signaling is well established (Bastos et al., 2015b; Michalareas et al., 2016), evidence linking α/β -band responses to prediction signals is limited (Arnal and Giraud, 2012). A recent human ECoG study, using a semi-predictable sequence of sounds to force the subjects to continuously update their predictions, provided the first direct evidence that β -band oscillations are involved in updating the content of sensory predictions (Sedley et al., 2016). Our results concur and further show that prediction updates are linked to a β -power decrease, which suggests that β -band oscillations are associated with the maintenance of predictions, and thus need to be removed or reduced when updates are required.

Limitations and Further Tests of the Theory

Here, we propose several future directions that could help further verify the predictive-coding theory, particularly at the mesoscopic level. One limitation of the present experiment is that it could not fully isolate the prediction signals, since predictions and prediction errors were always intertwined. Global prediction signals could only be identified by their change during the first 20 trials of a block. In the future, a more direct approach would be to systematically manipulate the local and global prediction strengths (see discussion below). Another useful strategy would be to probe the network response with omission trials (e.g., 4-tone sequence xxxx) (Wacongne et al., 2011), which could provide crucial information about the spontaneous timing of the prediction signals when no external stimuli are presented and allow us to examine the possible difference between an omitted error (e.g., $PE1x$) and an unpredicted error (e.g., $PE1Y$).

Another limitation is that our analysis only explored the functional correlation between prediction-error and prediction-update signals and thus cannot fully evaluate the causal links between the underlying processes. One analytical approach to further probe the relations between prediction and prediction-error signals across hierarchies would be to model the data with dynamic causal modeling (DCM) (Friston et al., 2003). DCM is a method designed to make and estimate inferences about the coupling among brain areas, which has been implemented to

reveal possible canonical circuits in the context of predictive coding (Aukstulewicz and Friston, 2015; Bastos et al., 2015a; Brown and Friston, 2012). A more direct experimental approach would be to systematically control local- and global-level prediction strengths by independently manipulating sequence length and sequence frequency. Furthermore, prediction strengths could be altered in a seamless manner using probabilistic rather than deterministic rules (Sedley et al., 2016). This would allow to examine how predictions and prediction errors are dynamically coupled, and to monitor how predictions at different hierarchies are established and altered by the sensory inputs.

Finally, to probe the proposed hierarchical cortical organization, additional experiments could vary the complexity of the regularities at larger temporal scales, using as a guideline the recently proposed hierarchy of sequence knowledge (Dehaene et al., 2015). More complex rules could, however, become significantly more difficult to detect. Other alternatives are using speech stimuli that introduce multi-level syntactic structures, visual stimuli in which hierarchical features can be more easily defined according to both their sequential and spatial configurations, or multi-modal audiovisual stimuli. Last but not least, in future work, the information content carried by the prediction signals should be assessed, for instance, by taking advantage of electrophysiological or optical methods for multiple single-unit recordings. To further understand predictive coding in the brain, it will be essential to decode the neural representations of predictions across hierarchies, which collectively could reveal how the brain encodes its internal models of the world.

In summary, our findings support the hierarchical predictive-coding theory by providing a high-resolution dynamic description of how prediction and prediction-error signals at different hierarchies interact with each other over distinct cortical areas and frequency bands. The combination of large-scale neuronal recordings with data-driven and hypothesis-driven analyses allows a systematic exploration of mesoscopic cortical dynamics, which provides potential target brain areas and communication channels for future mechanistic study of predictive coding, particularly, the study on how prediction and prediction-error signals are created at the cellular level and how they causally interact in microcircuits.

STAR★METHODS

Detailed methods are provided in the online version of this paper and include the following:

- **KEY RESOURCES TABLE**
- **CONTACT FOR REAGENT AND RESOURCE SHARING**
- **EXPERIMENTAL MODEL AND SUBJECT DETAILS**
 - Subjects and experimental setup
 - Electrode implant
 - Stimulus design and experimental protocol
 - Data analysis

SUPPLEMENTAL INFORMATION

Supplemental Information includes eight figures and two tables and can be found with this article online at <https://doi.org/10.1016/j.neuron.2018.10.004>.

ACKNOWLEDGMENTS

We thank Naomi Hasegawa and Tomonori Notoya for providing veterinary care and technical support. This work was supported by the Brain Science Project of the Center for Novel Science Initiatives (CNSI), National Institute of Natural Science (NINS; Grant Number BS261006), and Ministry of Education, Culture, Sports, Science, and Technology Grant in Aid for Scientific Research on Innovative Areas (21118002). S.D. was supported by Inserm, CEA, Collège de France, the Canadian Institute for Advanced Research (CIFAR), and the European Research Council (ERC).

AUTHOR CONTRIBUTIONS

Conceptualization, S.D. and Z.C.C.; Methodology, Z.C.C., S.D., L.W., and K.T.; Formal Analysis, Z.C.C.; Investigation, K.T. and Z.C.C.; Resources, N.F.; Writing – Original Draft, Z.C.C.; Writing – Review & Editing, Z.C.C., S.D., and K.T.; Visualization, Z.C.C.; Funding Acquisition, N.F. and S.D.

DECLARATION OF INTERESTS

The authors declare no competing interests.

Received: May 4, 2018

Revised: August 29, 2018

Accepted: October 2, 2018

Published: October 25, 2018

REFERENCES

- Akaike, H. (1974). A new look at the statistical model identification. *IEEE Trans. Automat. Contr.* *19*, 716–723.
- Alink, A., Schwiedrzik, C.M., Kohler, A., Singer, W., and Muckli, L. (2010). Stimulus predictability reduces responses in primary visual cortex. *J. Neurosci.* *30*, 2960–2966.
- Andersson, C.A., and Bro, R. (2000). The N-way toolbox for MATLAB. *Chemom. Intell. Lab. Syst.* *52*, 1–4.
- Arnal, L.H., and Giraud, A.-L. (2012). Cortical oscillations and sensory predictions. *Trends Cogn. Sci.* *16*, 390–398.
- Arnal, L.H., Wyart, V., and Giraud, A.-L. (2011). Transitions in neural oscillations reflect prediction errors generated in audiovisual speech. *Nat. Neurosci.* *14*, 797–801.
- Aukstulewicz, R., and Friston, K. (2015). Attentional enhancement of auditory mismatch responses: A DCM/MEG study. *Cereb. Cortex* *25*, 4273–4283.
- Barbas, H., Medalla, M., Alade, O., Suski, J., Zikopoulos, B., and Lera, P. (2005). Relationship of prefrontal connections to inhibitory systems in superior temporal areas in the rhesus monkey. *Cereb. Cortex* *15*, 1356–1370.
- Bastos, A.M., Usrey, W.M., Adams, R.A., Mangun, G.R., Fries, P., and Friston, K.J. (2012). Canonical microcircuits for predictive coding. *Neuron* *76*, 695–711.
- Bastos, A.M., Litvak, V., Moran, R., Bosman, C.A., Fries, P., and Friston, K.J. (2015a). A DCM study of spectral asymmetries in feedforward and feedback connections between visual areas V1 and V4 in the monkey. *Neuroimage* *108*, 460–475.
- Bastos, A.M., Vezoli, J., Bosman, C.A., Schoffelen, J.-M., Oostenveld, R., Dowdall, J.R., De Weerd, P., Kennedy, H., and Fries, P. (2015b). Visual areas exert feedforward and feedback influences through distinct frequency channels. *Neuron* *85*, 390–401.
- Beckmann, C.F., and Smith, S.M. (2005). Tensorial extensions of independent component analysis for multisubject fMRI analysis. *Neuroimage* *25*, 294–311.
- Bekinschtein, T.A., Dehaene, S., Rohaut, B., Tadel, F., Cohen, L., and Naccache, L. (2009). Neural signature of the conscious processing of auditory regularities. *Proc. Natl. Acad. Sci. USA* *106*, 1672–1677.
- Blank, H., and Davis, M.H. (2016). Prediction errors but not sharpened signals simulate multivoxel fMRI patterns during speech perception. *PLoS Biol.* *14*, e1002577.

- Brainard, D.H. (1997). The psychophysics toolbox. *Spat Vis.* 10, 433–436.
- Bressler, S.L., and Seth, A.K. (2011). Wiener-Granger causality: A well established methodology. *Neuroimage* 58, 323–329.
- Bro, R., and Kiers, H.A. (2003). A new efficient method for determining the number of components in PARAFAC models. *J. Chemometr.* 17, 274–286.
- Brodski, A., Paasch, G.-F., Helbling, S., and Wibral, M. (2015). The faces of predictive coding. *J. Neurosci.* 35, 8997–9006.
- Brovelli, A., Ding, M., Ledberg, A., Chen, Y., Nakamura, R., and Bressler, S.L. (2004). Beta oscillations in a large-scale sensorimotor cortical network: Directional influences revealed by Granger causality. *Proc. Natl. Acad. Sci. USA* 101, 9849–9854.
- Brown, H.R., and Friston, K.J. (2012). Dynamic causal modelling of precision and synaptic gain in visual perception - an EEG study. *Neuroimage* 63, 223–231.
- Chao, Z.C., Nagasaka, Y., and Fujii, N. (2010). Long-term asynchronous decoding of arm motion using electrocorticographic signals in monkeys. *Front. Neuroeng.* 3, 3.
- Chao, Z.C., Nagasaka, Y., and Fujii, N. (2015). Cortical network architecture for context processing in primate brain. *eLife* 4, e06121.
- Chao, Z.C., Sawada, M., Isa, T., and Nishimura, Y. (2018). Dynamic reorganization of motor networks during recovery from partial spinal cord injury in monkeys. *Cereb. Cortex*. Published online July 27, 2018. <https://doi.org/10.1093/cercor/bhy172>.
- Chen, J.L., Zatorre, R.J., and Penhune, V.B. (2006). Interactions of auditory and dorsal premotor cortex during synchronization to musical rhythms. *Neuroimage* 32, 1771–1781.
- Chen, J.L., Penhune, V.B., and Zatorre, R.J. (2008). Listening to musical rhythms recruits motor regions of the brain. *Cereb. Cortex* 18, 2844–2854.
- Chennu, S., Noreika, V., Gueorguiev, D., Blenkmann, A., Kochen, S., Ibáñez, A., Owen, A.M., and Bekinschtein, T.A. (2013). Expectation and attention in hierarchical auditory prediction. *J. Neurosci.* 33, 11194–11205.
- Cichocki, A., Zdunek, R., Phan, A.H., and Amari, S.-i. (2009). *Nonnegative Matrix and Tensor Factorizations: Applications to Exploratory Multi-Way Data Analysis and Blind Source Separation* (Wiley).
- Clark, A. (2013). Whatever next? Predictive brains, situated agents, and the future of cognitive science. *Behav. Brain Sci.* 36, 181–204.
- Curtis, C.E., and D'Esposito, M. (2003). Persistent activity in the prefrontal cortex during working memory. *Trends Cogn. Sci.* 7, 415–423.
- Dehaene, S., Meyniel, F., Wacongne, C., Wang, L., and Pallier, C. (2015). The neural representation of sequences: From transition probabilities to algebraic patterns and linguistic trees. *Neuron* 88, 2–19.
- Delorme, A., Sejnowski, T., and Makeig, S. (2007). Enhanced detection of artifacts in EEG data using higher-order statistics and independent component analysis. *Neuroimage* 34, 1443–1449.
- Delorme, A., Mullen, T., Kothe, C., Akalin Acar, Z., Bigdely-Shamlo, N., Vankov, A., and Makeig, S. (2011). EEGLAB, SIFT, NFT, BCILAB, and ERICA: New tools for advanced EEG processing. *Comput. Intell. Neurosci.* 2011, 130714.
- Ding, M., Bressler, S.L., Yang, W., and Liang, H. (2000). Short-window spectral analysis of cortical event-related potentials by adaptive multivariate autoregressive modeling: Data preprocessing, model validation, and variability assessment. *Biol. Cybern.* 83, 35–45.
- Dürschmid, S., Edwards, E., Reichert, C., Dewar, C., Hinrichs, H., Heinze, H.-J., Kirsch, H.E., Dalal, S.S., Deouell, L.Y., and Knight, R.T. (2016). Hierarchy of prediction errors for auditory events in human temporal and frontal cortex. *Proc. Natl. Acad. Sci. USA* 113, 6755–6760.
- Edwards, E., Soltani, M., Deouell, L.Y., Berger, M.S., and Knight, R.T. (2005). High gamma activity in response to deviant auditory stimuli recorded directly from human cortex. *J. Neurophysiol.* 94, 4269–4280.
- Egner, T., Monti, J.M., and Summerfield, C. (2010). Expectation and surprise determine neural population responses in the ventral visual stream. *J. Neurosci.* 30, 16601–16608.
- El Karoui, I., King, J.-R., Sitt, J., Meyniel, F., Van Gaal, S., Hasboun, D., Adam, C., Navarro, V., Baulac, M., and Dehaene, S. (2014). Event-related potential, time-frequency, and functional connectivity facets of local and global auditory novelty processing: An intracranial study in humans. *Cereb. Cortex* 25, 4203–4212.
- Eliades, S.J., and Wang, X. (2008). Neural substrates of vocalization feedback monitoring in primate auditory cortex. *Nature* 453, 1102–1106.
- Fontolan, L., Morillon, B., Liegeois-Chauvel, C., and Giraud, A.-L. (2014). The contribution of frequency-specific activity to hierarchical information processing in the human auditory cortex. *Nat. Commun.* 5, 4694.
- Fries, P. (2005). A mechanism for cognitive dynamics: Neuronal communication through neuronal coherence. *Trends Cogn. Sci.* 9, 474–480.
- Friston, K. (2005). A theory of cortical responses. *Philos. Trans. R. Soc. Lond. B Biol. Sci.* 360, 815–836.
- Friston, K. (2010). The free-energy principle: A unified brain theory? *Nat. Rev. Neurosci.* 11, 127–138.
- Friston, K.J., Harrison, L., and Penny, W. (2003). Dynamic causal modelling. *Neuroimage* 19, 1273–1302.
- Fukushima, M., Chao, Z.C., and Fujii, N. (2015). Studying brain functions with mesoscopic measurements: Advances in electrocorticography for non-human primates. *Curr. Opin. Neurobiol.* 32, 124–131.
- Gilbert, S.J., Spengler, S., Simons, J.S., Steele, J.D., Lawrie, S.M., Frith, C.D., and Burgess, P.W. (2006). Functional specialization within rostral prefrontal cortex (area 10): A meta-analysis. *J. Cogn. Neurosci.* 18, 932–948.
- Harshman, R.A., and Lundy, M.E. (1994). PARAFAC: Parallel factor analysis. *Comput. Stat. Data Anal.* 18, 39–72.
- Kamiński, M., Ding, M., Truccolo, W.A., and Bressler, S.L. (2001). Evaluating causal relations in neural systems: Granger causality, directed transfer function and statistical assessment of significance. *Biol. Cybern.* 85, 145–157.
- Keller, G.B., Bonhoeffer, T., and Hübner, M. (2012). Sensorimotor mismatch signals in primary visual cortex of the behaving mouse. *Neuron* 74, 809–815.
- Kiers, H.A. (1991). Hierarchical relations among three-way methods. *Psychometrika* 56, 449–470.
- Kok, P., Jehee, J.F., and de Lange, F.P. (2012). Less is more: Expectation sharpens representations in the primary visual cortex. *Neuron* 75, 265–270.
- Kroonenberg, P.M. (1983). *Three-Mode Principal Component Analysis: Theory and Applications* Volume 2 (DSWO Press).
- Lima, C.F., Krishnan, S., and Scott, S.K. (2016). Roles of supplementary motor areas in auditory processing and auditory imagery. *Trends Neurosci.* 39, 527–542.
- Maris, E., and Oostenveld, R. (2007). Nonparametric statistical testing of EEG- and MEG-data. *J. Neurosci. Methods* 164, 177–190.
- Medalla, M., and Barbas, H. (2014). Specialized prefrontal “auditory fields”: Organization of primate prefrontal-temporal pathways. *Front. Neurosci.* 8, 77.
- Meister, I.G., Wilson, S.M., Deblieck, C., Wu, A.D., and Iacoboni, M. (2007). The essential role of premotor cortex in speech perception. *Curr. Biol.* 17, 1692–1696.
- Meyniel, F., Maheu, M., and Dehaene, S. (2016). Human inferences about sequences: A minimal transition probability model. *PLoS Comput. Biol.* 12, e1005260.
- Michalareas, G., Vezoli, J., van Pelt, S., Schoffelen, J.-M., Kennedy, H., and Fries, P. (2016). Alpha-beta and gamma rhythms subserve feedback and feedforward influences among human visual cortical areas. *Neuron* 89, 384–397.
- Miwakeichi, F., Martínez-Montes, E., Valdés-Sosa, P.A., Nishiyama, N., Mizuhara, H., and Yamaguchi, Y. (2004). Decomposing EEG data into space-time-frequency components using Parallel Factor Analysis. *Neuroimage* 22, 1035–1045.
- Morillon, B., and Baillet, S. (2017). Motor origin of temporal predictions in auditory attention. *Proc. Natl. Acad. Sci. USA* 114, E8913–E8921.
- Mørup, M., Hansen, L.K., Herrmann, C.S., Parnas, J., and Arnfred, S.M. (2006). Parallel Factor Analysis as an exploratory tool for wavelet transformed event-related EEG. *Neuroimage* 29, 938–947.

- Mumford, D. (1992). On the computational architecture of the neocortex. II. The role of cortico-cortical loops. *Biol. Cybern.* *66*, 241–251.
- Nagasaka, Y., Shimoda, K., and Fujii, N. (2011). Multidimensional recording (MDR) and data sharing: An ecological open research and educational platform for neuroscience. *PLoS ONE* *6*, e22561.
- Oostenveld, R., Fries, P., Maris, E., and Schoffelen, J.-M. (2011). FieldTrip: Open source software for advanced analysis of MEG, EEG, and invasive electrophysiological data. *Comput. Intell. Neurosci.* *2011*, 156869.
- Pelli, D.G. (1997). The VideoToolbox software for visual psychophysics: Transforming numbers into movies. *Spat Vis.* *10*, 437–442.
- Pulvermüller, F., and Fadiga, L. (2010). Active perception: Sensorimotor circuits as a cortical basis for language. *Nat. Rev. Neurosci.* *11*, 351–360.
- Quattrocki, E., and Friston, K. (2014). Autism, oxytocin and interoception. *Neurosci. Biobehav. Rev.* *47*, 410–430.
- Rao, R.P., and Ballard, D.H. (1999). Predictive coding in the visual cortex: A functional interpretation of some extra-classical receptive-field effects. *Nat. Neurosci.* *2*, 79–87.
- Romanski, L.M., and Averbeck, B.B. (2009). The primate cortical auditory system and neural representation of conspecific vocalizations. *Annu. Rev. Neurosci.* *32*, 315–346.
- Schubotz, R.I. (2007). Prediction of external events with our motor system: Towards a new framework. *Trends Cogn. Sci.* *11*, 211–218.
- Schubotz, R.I., von Cramon, D.Y., and Lohmann, G. (2003). Auditory what, where, and when: A sensory somatotopy in lateral premotor cortex. *Neuroimage* *20*, 173–185.
- Sedley, W., Gander, P.E., Kumar, S., Kovach, C.K., Oya, H., Kawasaki, H., Howard, M.A., III, and Griffiths, T.D. (2016). Neural signatures of perceptual inference. *eLife* *5*, e11476.
- Srinivasan, M.V., Laughlin, S.B., and Dubs, A. (1982). Predictive coding: A fresh view of inhibition in the retina. *Proc. R. Soc. Lond. B Biol. Sci.* *216*, 427–459.
- Stephan, K.E., Friston, K.J., and Frith, C.D. (2009). Dysconnection in schizophrenia: From abnormal synaptic plasticity to failures of self-monitoring. *Schizophr. Bull.* *35*, 509–527.
- Strauss, M., Sitt, J.D., King, J.-R., Elbaz, M., Azizi, L., Buiatti, M., Naccache, L., van Wassenhove, V., and Dehaene, S. (2015). Disruption of hierarchical predictive coding during sleep. *Proc. Natl. Acad. Sci. USA* *112*, E1353–E1362.
- Summerfield, C., and Koechlin, E. (2008). A neural representation of prior information during perceptual inference. *Neuron* *59*, 336–347.
- Summerfield, C., Egner, T., Greene, M., Koechlin, E., Mangels, J., and Hirsch, J. (2006). Predictive codes for forthcoming perception in the frontal cortex. *Science* *314*, 1311–1314.
- Tallon-Baudry, C., and Bertrand, O. (1999). Oscillatory gamma activity in humans and its role in object representation. *Trends Cogn. Sci.* *3*, 151–162.
- Todorovic, A., van Ede, F., Maris, E., and de Lange, F.P. (2011). Prior expectation mediates neural adaptation to repeated sounds in the auditory cortex: An MEG study. *J. Neurosci.* *31*, 9118–9123.
- Uhrig, L., Dehaene, S., and Jarraya, B. (2014). A hierarchy of responses to auditory regularities in the macaque brain. *J. Neurosci.* *34*, 1127–1132.
- van Kerkoerle, T., Self, M.W., Dagnino, B., Gariel-Mathis, M.-A., Poort, J., van der Togt, C., and Roelfsema, P.R. (2014). Alpha and gamma oscillations characterize feedback and feedforward processing in monkey visual cortex. *Proc. Natl. Acad. Sci. USA* *111*, 14332–14341.
- Wacongne, C., Labyt, E., van Wassenhove, V., Bekinschtein, T., Naccache, L., and Dehaene, S. (2011). Evidence for a hierarchy of predictions and prediction errors in human cortex. *Proc. Natl. Acad. Sci. USA* *108*, 20754–20759.
- Wang, X.-J. (2010). Neurophysiological and computational principles of cortical rhythms in cognition. *Physiol. Rev.* *90*, 1195–1268.
- Wang, L., Uhrig, L., Jarraya, B., and Dehaene, S. (2015). Representation of numerical and sequential patterns in macaque and human brains. *Curr. Biol.* *25*, 1966–1974.
- Wilson, B., Marslen-Wilson, W.D., and Petkov, C.I. (2017). Conserved sequence processing in primate frontal cortex. *Trends Neurosci.* *40*, 72–82.
- Yanagawa, T., Chao, Z.C., Hasegawa, N., and Fujii, N. (2013). Large-scale information flow in conscious and unconscious states: An ECoG study in monkeys. *PLoS ONE* *8*, e80845.
- Zatorre, R.J., Chen, J.L., and Penhune, V.B. (2007). When the brain plays music: Auditory-motor interactions in music perception and production. *Nat. Rev. Neurosci.* *8*, 547–558.

STAR★METHODS

KEY RESOURCES TABLE

REAGENT or RESOURCE	SOURCE	IDENTIFIER
Software and Algorithms		
MATLAB	Mathworks	https://www.mathworks.com
Psychophysics Toolbox	(Brainard, 1997; Pelli, 1997)	
EEGLAB Toolbox	(Delorme et al., 2011)	https://sccn.ucsd.edu/eeglab/index.php
FieldTrip Toolbox	(Oostenveld et al., 2011)	http://www.fieldtriptoolbox.org/
Source Information Flow Toolbox (SIFT)	(Delorme et al., 2011)	https://sccn.ucsd.edu/wiki/SIFT
N-way Toolbox	(Andersson and Bro, 2000)	http://www.models.life.ku.dk/nwaytoolbox

CONTACT FOR REAGENT AND RESOURCE SHARING

Further information and requests should be directed to and will be fulfilled by the Lead Contact Dr. Zenas C. Chao (zenas.c.chao@gmail.com).

EXPERIMENTAL MODEL AND SUBJECT DETAILS

Subjects and experimental setup

Two macaque monkeys, identified as Subjects 1 (male, 8.8 kg) and 2 (male, 7.5 kg), were used in the experiments after brain MRIs were acquired. Before the monkeys were implanted with subdural ECoG electrodes, they were familiarized with the experimental environment. The monkeys were seated in a primate chair in a dark, electrically shielded and sound-attenuated chamber with their head fixed in a position with a custom-made helmet. A custom-made eye-tracking system was used for monitoring the monkey's right eye with a 30 Hz sampling rate (Nagasaka et al., 2011). Cerebus data acquisition systems (Blackrock Microsystems, USA) were used to record ECoG signals with a sampling rate of 1 kHz. An iMac personal computer (Apple, USA) was used to present the fixation point on a 24-in LCD monitor located 60 cm away from the subject, and the same PC was used to record monkey's gaze and neural signals via USB-1208LS data acquisition device (Measurement Computing Co., USA). For auditory stimuli, we positioned a pair of audio speakers (Fostex, Japan) on the right and left sides, at a distance of ~80 cm from the head. We used MATLAB (Mathworks, Natick, MA, USA) and Psychophysics Toolbox (Brainard, 1997; Pelli, 1997) to present auditory stimuli.

Electrode implant

Subdural electrodes were surgically implanted. The monkeys were anesthetized by administration of atropine (0.05 mg/kg, intramuscular), ketamine (5 mg/kg, intramuscular) and pentobarbital (20 mg/kg, intravenous). Throughout surgery we monitored the heart rate, blood pressure, body temperature, SpO₂ (peripheral capillary oxygen saturation), and reflex response to noxious stimulation, adjusting the dose of pentobarbital accordingly. In the subdural space we chronically implanted customized 128-channel ECoG electrode arrays (Unique Medical, Japan) containing 2.1 mm diameter platinum electrodes (1 mm diameter exposed from a silicone sheet) with an inter-electrode distances of 5 mm). In Subject 1, electrodes were placed to cover most of the lateral surface of the right hemisphere, also under the orbitofrontal lobe. In Subject 2, all electrodes were placed on the lateral surface of the right hemisphere, and no orbitofrontal part was covered. In both subjects, a reference electrode was implanted in the subdural space and a ground electrode was implanted in the epidural space above the right hemisphere (the reference and ground electrodes were 5-mm x 10-mm rectangular platinum plates). Electrical cables leading from the ECoG electrodes were connected to Omnetics connectors (Unique Medical) affixed to the skull with an adaptor and titanium screws. To localize the electrodes, we acquired post-operative X-ray images and co-registered them with the MRIs. We manually identified the location of each electrode by projecting the electrodes in the X-ray images onto the cortical surface reconstructed from the MRIs.

All experimental and surgical procedures were performed in accordance with the experimental protocols (No. H24-2-203(4)) approved by the RIKEN ethics committee and the recommendations of the Weatherall report, 'The use of non-human primates in research'. Implantation surgery was performed under sodium pentobarbital anesthesia, and all efforts were made to minimize suffering. No animal was sacrificed in this study. Overall care was managed by the Division of Research Resource Center at RIKEN Brain Science Institute. The animal was housed in a large individual enclosure with other animals visible in the room, and maintained on a 12:12-hr light:dark cycle. The animal was given food (PS-A; Oriental Yeast Co., Ltd., Tokyo, Japan) and water *ad libitum*, and also

daily fruit/dry treats as a means of enrichment and novelty. The animal was occasionally provided toys in the cage. The in-house veterinary doctor checked the animal and updated daily feedings in order to maintain weight. We have attempted to offer as humane treatment of our subject as possible.

Stimulus design and experimental protocol

Two tones with different pitches (Tone A = 500Hz; Tone B = 1280Hz) were synthesized. Each tone was 50 ms in duration with 7 ms rise and fall times (average intensity 65 dB SPL). Series of five tones were presented with a 150 ms inter-tone interval, with 200~300 ms between the fixation onset and the first tone onset and more than 600 ms between the last tone onset and the fixation offset. Thus, the subject was required to maintain fixation 1.6~1.7 s for each trial.

Four different stimulus blocks were used: AAAAA, BBBBB, AAAAB, and BBBBA blocks. In AAAAA blocks, 20 AAAAA sequences were delivered, followed by a random mixture of 80 AAAAA and 20 AAAAB. In BBBBB blocks, 20 BBBBB sequences were delivered, followed by a random mixture of 80 BBBBB and 20 BBBBA. In AAAAB blocks, 20 AAAAB sequences were delivered, followed by a random mixture of 80 AAAAB and 20 AAAAA. In BBBBA blocks, 20 BBBBA sequences were delivered, followed by a random mixture of 80 BBBBA and 20 BBBBB. In average, each block took ~6.5 min to finish, and one session of experiment consisted of four blocks delivered in a randomized order (~30 min). Two sessions of experiments were performed on each experimental day, with rewards and break given in between. Experimental data were obtained over 4 experiments for both subjects (4 experiments in 13 days for Subject 1, an in 7 days for Subject 2). In total, we recorded ECoG signals for 8 sessions in each monkey.

Data analysis

Preprocessing

For each trial, the ECoG signals were aligned at the onset of the first tone, and signals from 0.5 s before to 1.7 s after the onset of the first tone (-0.5~1.7 s) were segmented and used for the further analyses. The signals were then downsampled 4 times, resulted in a sampling rate of 250Hz. Trials with abnormal spectra were rejected by using an automated algorithm (MATLAB function: `pop_rejspec.m`) from the EEGLAB library (Delorme et al., 2011), which has been suggested as the most effective method for artifact rejection (Delorme et al., 2007). After removing the artifactual trials, the 50Hz line noise was removed from the data. The data was further re-referenced using a common average reference (CAR) montage, detrended to remove the linear drift in the data, and demeaned to remove the temporal mean. The re-referencing, CAR, detrend, and demean were done using the MATLAB FieldTrip toolbox (`ft_preprocessing.m`) (Oostenveld et al., 2010).

Activity analysis

Wavelet transformation: Time-frequency representation (TFR) of the ECoG signals for each electrode was generated by Morlet wavelet transformation at 110 different center frequencies (10~120Hz) with the half-length of the Morlet analyzing wavelet set at the coarsest scale of 5 samples, which is implemented in FieldTrip Toolbox (`ft_freqanalysis.m`). To further quantify induced responses, the novelty responses phase-locked to the stimuli ("evoked" responses) were removed by averaging ECoG signals in each trial type, and subtracting the TFRs of these phase-locked evoked responses from the TFRs of the overall responses (Tallon-Baudry and Bertrand, 1999). Evoked responses were removed from the further analysis.

Comparisons of activity

To evaluate the significant differences in TFRs in each comparison, we performed permutations by shuffling trial indices, and used a nonparametric cluster-based method for multiple comparisons correction (Maris and Oostenveld, 2007), which is implemented in FieldTrip Toolbox (`ft_freqstatistics.m`). For each permutation, independent sample t tests were performed at each time and frequency sample, and samples with a p value smaller than 0.05 were clustered in if they were next to each other in the time-frequency space. The cluster-level statistic was calculated as the sum of the t-statistics within each cluster, and the maximum of the cluster-level statistics is taken as the test statistic for the permutation. A histogram of test statistics was constructed from 500 permutations, and the cluster-corrected threshold for significance was determined as the test-statistic where the proportion of permutations with greater test statistics (the Monte Carlo significance probability) was 0.05. The cluster-level statistic was also calculated from the original unshuffled data, and clusters with a cluster-level statistic greater than the threshold were identified as significant.

Connectivity analysis

Three preparation steps were performed for the spectral GC calculation: (1). *Preprocessing*: detrending, temporal normalization, and ensemble normalization were performed to achieve local stationarity of the data (Ding et al., 2000), and were implemented in FieldTrip toolbox (`ft_preprocessing.m`). Detrending, which is the subtraction of the best-fitting line from each time series, removes the linear drift in the data. Temporal normalization, which is the subtraction of the mean of each time series and division by the standard deviation, ensures that all variables have equal weights across the trial. These processes were performed on each trial for each channel. Ensemble normalization, which is the pointwise subtraction of the ensemble mean and division by the ensemble standard deviation, dramatically improves the local stationarity of the data (Bressler and Seth, 2011; Ding et al., 2000). (2). *Window length selection*: the length and the step size of the sliding-window for segmentation were set as 250 ms and 50 ms, respectively. (3). *Model order selection*: the model order, which is related to the length of the signal in the past that is relevant to the current observation, was determined by the Akaike information criterion (AIC) (Akaike, 1974) using the Source Information Flow Toolbox (SIFT) (`pop_est_selModelOrder.m`) (Delorme et al., 2011). In both subjects, a model order of 10 samples (equivalent to $10 \times 4 = 40$ ms of history) resulted in minimal AIC and was selected. The selected model order also passed the Kwiatkowski-Phillips-Schmidt-Shin (KPSS) test, thus maintaining local

stationarity (`pop_est_validateMVAR.m`). Furthermore, the vector autoregression (VAR) model was validated by the whiteness test and the consistency test (`est_checkMVARWhiteness.m` and `est_checkMVARConsistency.m`, respectively).

Comparisons of connectivity

Similar to the method used for activity comparison, we performed 500 permutations and used a nonparametric cluster-based method to determine the significant differences in spectral GC in each comparison. For each permutation, the shuffled data were preprocessed and spectral GC was measured, and the test statistic (the maximum of the cluster-level summed t-statistics) was calculated. The cluster-level statistic was also calculated from the original unshuffled data, and clusters with a cluster-level statistic greater than the threshold (Monte Carlo significance probability of 0.05) were identified as significant.

Parallel factor analysis (PARAFAC)

PARAFAC was performed by using the N-way toolbox (`parafac.m`) (Andersson and Bro, 2000), with the non-negativity constraint on the Anatomy dimension, and no constraints on other two dimensions. The convergence criterion, i.e., the relative change in fit for which the algorithm stops, was set to be $1e-6$. The initialization method was set to be DTLD (direct trilinear decomposition), which was considered the most accurate method (Cichocki et al., 2009). To determine the number of structures hidden in the dataset, we performed the core consistency diagnostic (CORCONDIA) to identify the appropriate latent structures where adding other latent structures does not considerably improve the model fit (Bro and Kiers, 2003).